Journal of the Serbian Society for Computational Mechanics / Vol. 18 / No. 2, 2024 / pp 62-76 / original paper
(10.24874/jsscm.2024.18.02.04)

A NEW DESIGN OF EFFICIENT PLANE SOLAR COLLECTORS FOR AIR AND WATER HEATING

Seyyed Abdolreza Gandjalikhan Nassab [0000-0003-0783-3155]

Shahid Bahonar University of Kerman, Mechanical Engineering Department, Kerman, Iran
e-mail: ganj110@uk.ac.ir

Abstract

In this paper, a new design of solar air-water heater for the purpose of performance improvement is introduced for the first time. This thermal system will be a good alternative for both space heating and providing domestic hot water for use in buildings. In the proposed solar collector, the absorbed incoming solar irradiation is transferred into both air and water flows. In numerical simulations, the governing equations for turbulent forced convection airflow with the conduction equation for glass cover, absorber plate, water tubes, and insulation are solved by means of the finite element method using the COMSOL Multiphysics software. In the studied test cases, from the total absorbed thermal energy by the absorber, about 18% is transferred to the airflow and 50% into the water flow. The effects of solar heat flux and the diameter of water tubes are also studied in this paper and thermal efficiency shows an increasing trend as the values of these parameters increase. A comparison of the thermal efficiencies between the designed solar air-water heater and a conventional solar air heater under the same operating conditions shows an increase of over 50%.

Keywords: solar air-water heater, efficiency, CFD, turbulence

1. Introduction

Solar air heaters (SAHs) play a key role in converting solar radiation into air enthalpy, although they are inexpensive heat exchangers with simple geometries. The plane SAHs come in different types and configurations and cover a wide range of low to moderate temperature-applications, including drying, cooking, air conditioning systems, etc. (Kalogirou, 2004; Aramesh, 2019). However, their low thermal performances due to low thermal conductivity of the working gas made these heat exchangers less attractive and inefficient. Many research papers have been published on this issue, proposing the ideas such as designing concave and convex airflow channels (Sigh, 2019), using porous medium and wire-mesh packed beds (Sigh, 2020), using extended surfaces such as ribs and internal multiple-fin array (Gandhi, 2010; Mems, 2016), employing vortex generation technique with passive and active methods (Sheihknejad, 2021), using radiant gases instead of air inside a closed loop (Forouzan Nia, 2020; Rayeni, 2020), as well as new geometries of arched and airfoil shaped absorber plates (Singh, 2017; Gandjalikhan Nassab, 2022), and also replacing a flat plate absorber with a V-groove one (Desisa, 2020; Ho, 2017). An experimental and thermodynamic analysis of a solar air dryer equipped with a V-groove double pass collector carried out by Hassan (2022), and the positive effect of absorber shape on convection enhancement was proven. Recently, the author proposed the use of converging air ducts in the construction of SAH for performance improvement (Gandjalikhan Nassab, 2022). In that CFD-based study, the flow and energy equations were solved numerically to obtain the thermo-hydrodynamic characteristics of the solar collector, and it was revealed that the acceleration of air through the converged air duct leads to convection enhancement. Regarding these methods for convection augmentation, SAHs have the potential to achieve higher efficiency. It is worth mentioning that the low air thermal conductivity also leads to high temperatures for the absorber plate and more heat transfer irreversibility. This undesired problem and low rate of heat transfer in SAHs motivated the author to combine the air and water solar heaters together and design a new type of solar air-water heater (SAWH) by installing the water tubes under the absorber plate perpendicular to the airflow as shown in Fig. 1. Using this technique and considering the higher density and thermal conductivity of water relative to air, a considerable amount of the radiative energy absorbed by the plate can be transferred into the water flow via the thin and conductive tube walls. Thus, in the present work, a theoretical investigation is made int the potential of the proposed design solution to change the destiny of this type of renewable solar-thermal system and to receive more attention from industrial applications. To reach this goal, the current study introduces a CFD-based numerical simulation of the proposed SWAH by a two-dimensional simultaneous solution of the governing equations. In the analysis, the convection coefficient of the water flow in pipes and the temperature of the working water, defined as the boundary conditions on the inner tube surface, are considered known parameters, such that the water flow is not simulated. The convection coefficient of water flow is obtained based on the mean values of the Nusselt number in fully developed flow for the constant wall temperature (Nu=3.66) and constant heat flux (Nu=4.36) cases.

2. Physical model

A schematic of the simulated plane SAWH, including the glass cover, air channel, absorber (including the absorber plate with the water tubes), and the insulation layer is described in Fig. 1. As shown, five tubes with semi-circular cross sections with the inner and outer diameters of 40 mm and 48 mm, respectively, are installed below the absorber plate. The water tubes are designed to have a common large surface area with the absorber plate for more convection heat transfer with the heated plate. The values of some geometrical parameters are reported in Table. 1. The water flows in tubes that are perpendicular to the air convection flow. Forced convection airflow enters the heater duct with the height of b=4 cm, whose value of the Reynolds number defined as $\rho\bar{V}D_h/\mu$ is equal to 2800, corresponding to an average inlet air velocity of 0.5 m/s ($\dot{m} = 0.024\ kg/s$) in all of the studied test cases. The outer surfaces of SAWH are exposed to convection and surface radiation with equivalent heat transfer coefficient, h_{eq} including both radiation and convection parts (Tan, 2016).

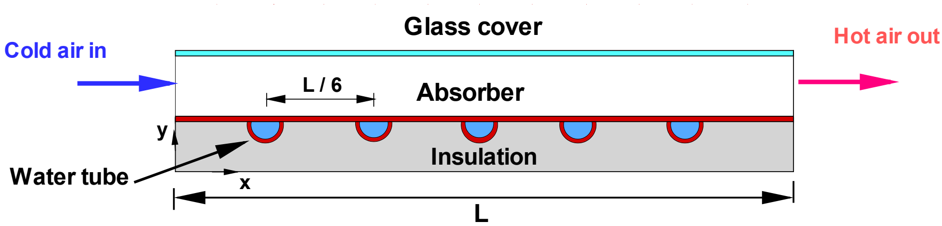

Fig. 1. Geometry of the proposed SAWH.

In order to obtain accurate and reliable numerical results, all thermo-physical properties of air are considered temperature-dependent. As mentioned before, the interior of the water tube is out of the computational domain and convection boundary condition with $h_w = 60 \frac{W}{m^2 K}, T_w = 320\ K$ is imposed on the interface surface. Therefore, only the airflow is simulated in the present study.

Physical properties	Insulation layer	Glass sheet	Absorber plate	Water tubes
Length [mm]	1000	1000	1000	-
Thickness[mm]	40	4	4	4
Surface emissivity	-	0.9	0.95	0.98
Reflectivity	-	0.03	0.03	-
Transmissivity	0	0.95	0	0
Conductivity [W/m.K]	0.04	0.8	390	390

Table 1. Some thermo-physical properties of solar collector.

3. Governing equations

All of the equations governing the airflow including the continuity, momentum, and energy equations for steady, incompressible turbulent flow with the standard $k - \varepsilon$ model in calculation of turbulent stresses and heat fluxes based on the RANS method may be expressed in the following tensor notation form (Sigh, 2019) and Launder, 1974):

Continuity:

$$\frac{\partial u_i}{\partial x_i} = 0 \tag{1}$$

Two-equation model for velocity field:

$$u_j \frac{\partial u_i}{\partial x_j} = -\frac{1}{\rho}\frac{\partial p}{\partial x_i} + \frac{\partial}{\partial x_j}[\nu(\frac{\partial u_i}{\partial x_j} + \frac{\partial u_j}{\partial x_i}) - \overline{u_i^{'} u_j^{'}}] \tag{2}$$

$$u_j \frac{\partial \kappa}{\partial x_j} = \frac{\partial}{\partial x_j}[(\nu + \frac{\nu_t}{\sigma_k})\frac{\partial \kappa}{\partial x_j}] - \overline{u_i^{'} u_j^{'}}\frac{\partial u_i}{\partial x_j} - \varepsilon \tag{3}$$

$$u_j \frac{\partial \varepsilon}{\partial x_j} = \frac{\partial}{\partial x_j}[(\nu + \frac{\nu_t}{\sigma_\varepsilon})\frac{\partial \varepsilon}{\partial x_j}] - C_{\varepsilon 1}\frac{\varepsilon}{\kappa}\overline{u_i^{'} u_j^{'}}\frac{\partial u_i}{\partial x_j} - C_{\varepsilon 2} f_\varepsilon \frac{\varepsilon^2}{\kappa} \tag{4}$$

where

$$-\overline{u_i' u_j'} = \nu_t \left(\frac{\partial u_i}{\partial x_j} + \frac{\partial u_j}{\partial x_i}\right) - \frac{2}{3} k \delta_{ij} \tag{5}$$

Energy equation:

$$u_j \frac{\partial T}{\partial x_j} = \frac{\partial}{\partial x_j}\left(\alpha \frac{\partial T}{\partial x_j} - \overline{u_j^{'} T^{'}}\right) \tag{6}$$

More details about the applied turbulence model and the values of constant in the above equations are given in Sigh (2019) and Launder (1974). The results from the grid study are reported in Table 2, in which the values of maximum temperature at five different grids with 12980 to 26930 elements are recorded. The grid with 22440, as shown in Fig. 3, is identified as the optimal one.

No. of elements	T_{max}	Variation with respect to the previous step
12980	352.3	-
15580	338.9	3.8%
18700	332.6	1.8%
22440	**329.3**	**1%**
26930	328.1	0.3%

Table 2. Mesh study.

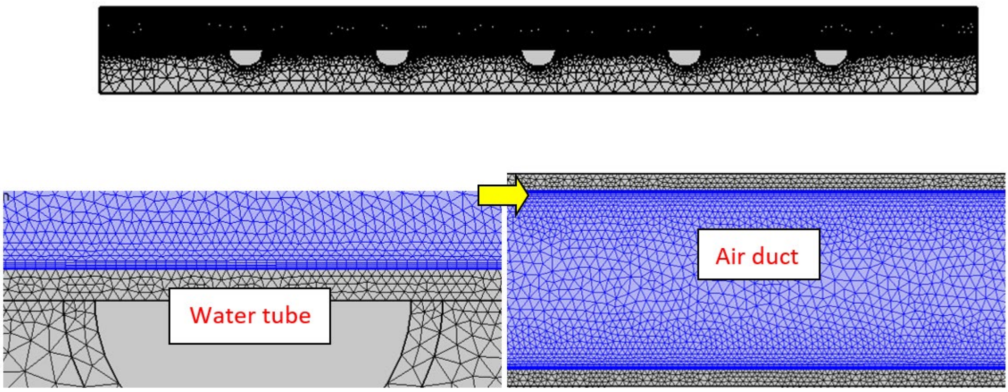

Fig. 2. The unstructured grid nodes with the triangular shape.

The obtained numerical solution and the applied physical model have been experimentally validated (Chabane, 2018). The plane SAH, which was studied experimentally, is analyzed here and the numerical findings are compared with experimental data. The efficiency of SAH, evaluated during the sunny day of the experiment from 9 AM to 2 PM, is plotted in Fig. 3. This figure shows high value for collector efficiency when it operated at a high air mass flow rate. However, Fig. 3 also indicates that there is a good consistency between the present numerical results and experimental data.

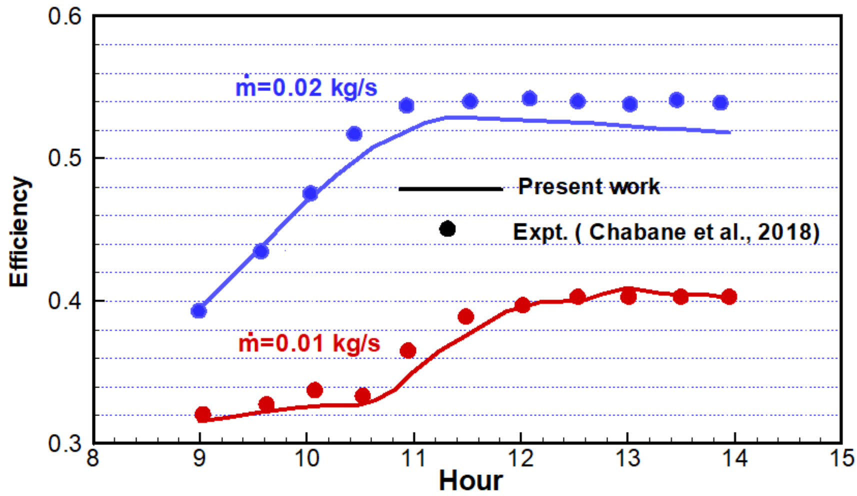

Fig. 3. The SAH efficiency at different hours.

4. Results and discussion

The thermal and hydraulic behavior of the proposed SAWH shown in Fig. 1 are discussed in this section, and the performance of this new type of solar collector is compared with a simple plane SAH under the same operating conditions. In all of the test cases, the average air velocity at the inlet section is equal to 0.75 m/s, the solar heat flux is in the range from 500 to 1100 W/m^2, and the temperature of the water flow and its convection coefficient are 320 K and 60 W/m^2K, respectively. At first, the flow behavior of SAWH is demonstrated in Fig. 4 by plotting the air velocity, pressure, and turbulent kinetic energy contours. About the velocity field, it is seen that air enters the heater with a fully developed profile such that the air velocity increases along the axial direction due to decreasing density as the convection flow is heated and its temperature rises. Figure 4-b demonstrates a small air pressure drop (less than 1 Pa) along the heater duct because of the friction. The contour plot of turbulent kinetic energy in Fig. 4-c depicts a high value of this parameter close to the boundary walls inside the boundary layer and a small value at the vicinity of the center line.

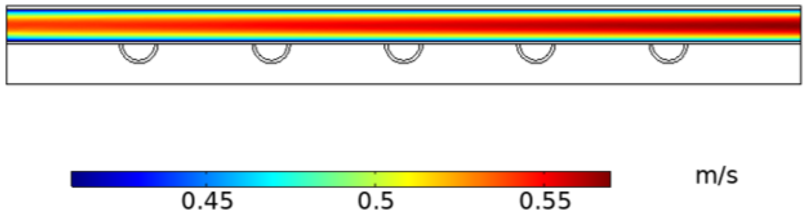

a) Contours of air velocity magnitude.

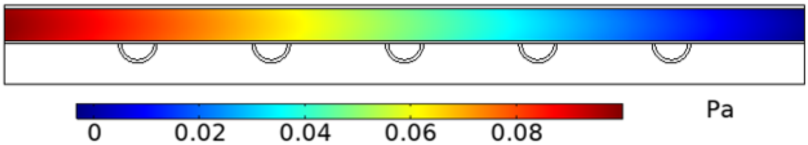

b) Contours of air pressure.

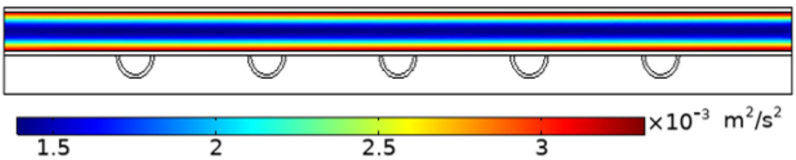

c) Contours of air turbulent kinetic energy.

Fig. 4. The contour plots of air velocity magnitude, pressure, and turbulent kinetic energy.

To demonstrate the thermal behavior of the simulated SAWH, the air temperature contour plot is presented in Fig. 5 for four different values of the solar heat flux. The maximum temperature occurs at the absorber plate where the incoming solar irradiation is absorbed. Inside the insulation layer closed to the heated absorber, the temperature is also high. Figure 5 shows how the air convection flow is heated as it passes through the air duct of the heater. The absorber plate including the water tubes behaves as an isothermal element due to high thermal conductivity. As observed, the heat penetration from the absorber surface into the airflow only occurs across a thin adjacent layer, and this is the main factor contributing to the low performance of the solar air heater. A comparison between the isotherm plots in Fig. 5 shows how the SAWH is affected by the incoming solar irradiation, such that the temperature pattern remains the same. However, the temperature across the entire SAWH domain increases significantly with an increase in solar heat flux.

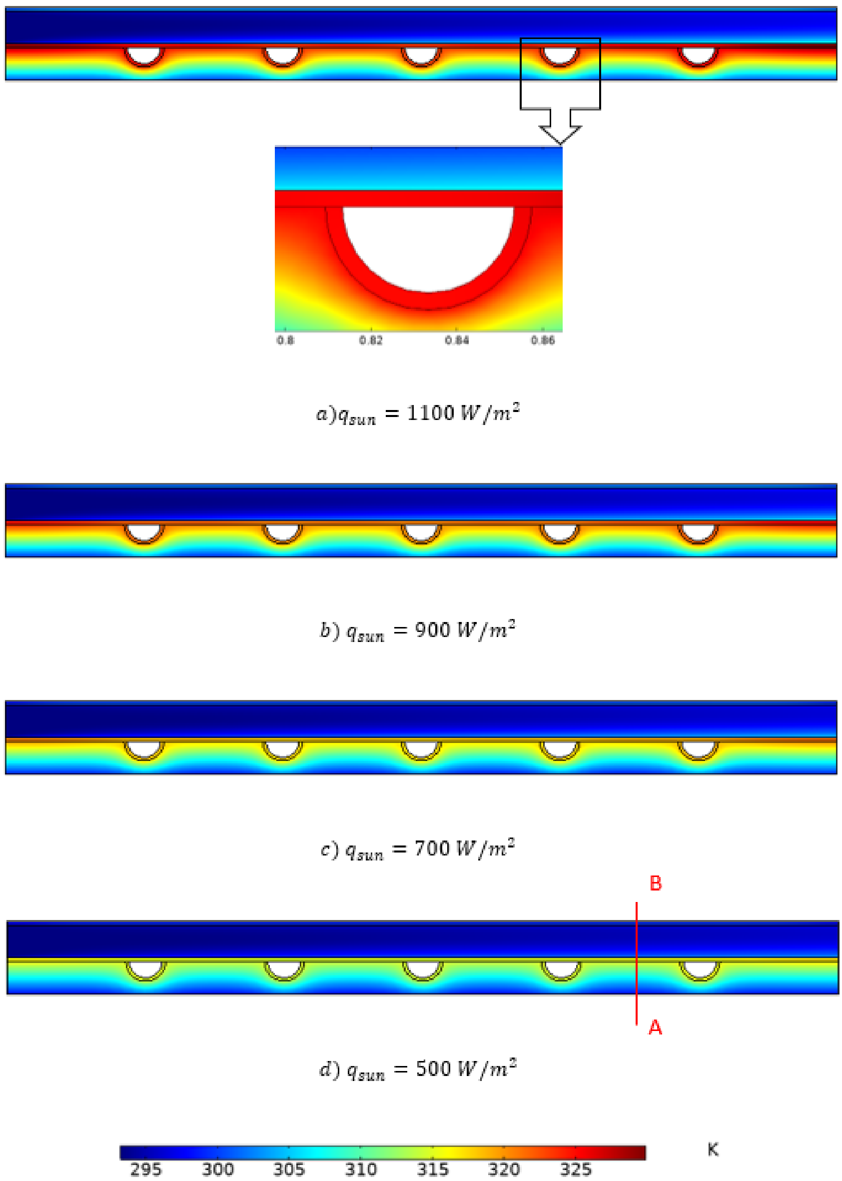

Fig. 5. Temperature contours for different degrees of incoming sun heat flux.

In Fig. 6, the temperature variations across the SAWH including the insulation, absorber, air duct, and glass cover at the axial section x=0.75L (along the line AB shown in Fig. 5-d) are plotted at different values of the solar heat flux. This figure effectively illustrates the thermal behavior of the collector. As observed, the temperature variation across the insulation layer has almost a linear trend, while the absorber behaves as a lumped system. The air temperature increase only occurs across a thin layer adjacent to the heated surface, and finally the glass temperature variation indicates almost a linear and decreasing trend. The same temperature pattern is seen in all parts of the collector but with higher values as the solar heat flux increases.

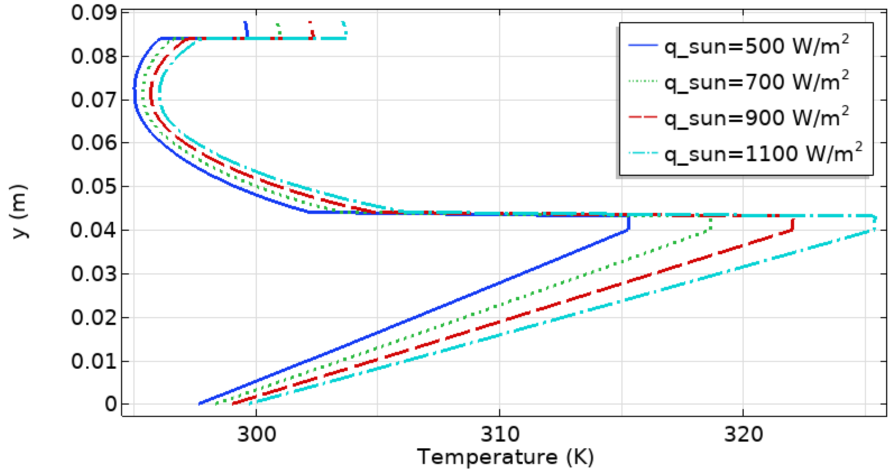

Fig. 6. Temperature variation across the SAWH at x=0.75 m.

The temperature distributions on the absorber surface as a main element of the SAWH are drawn in Fig. 7 for different values of the solar heat flux. The wavy form of curves plotted in this figure is due to the water tubes and their cooling effect, which are installed under the absorber plate. Based on Fig. 7, the minimum temperature occurs in the middle of the absorber and among the water tubes through which the cold fluid with high convection coefficient is passing. Besides, as expected, the absorber temperature increases as the incoming solar radiation reaches higher values.

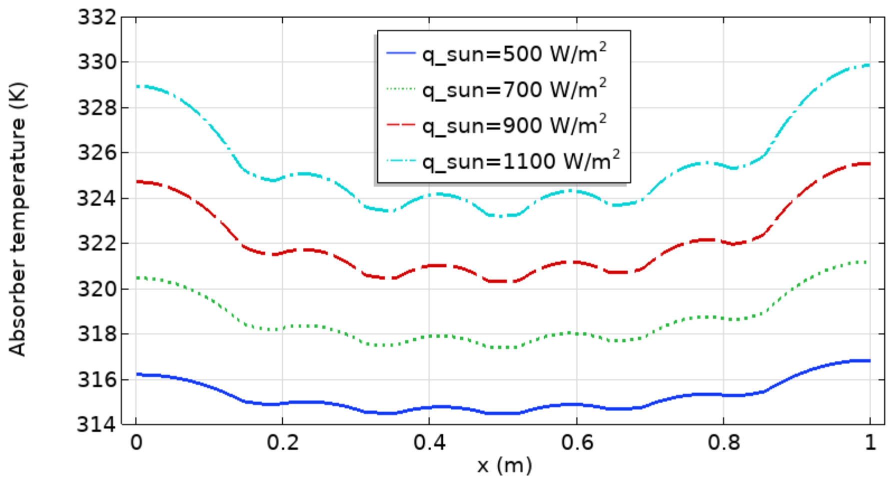

Fig. 7. Temperature variation along the upper surface of the absorber.

The effect of water tube diameter on the performance of the proposed SAWH is also examined in this work, and the temperature contours inside the collector at three different values of this parameter are plotted in Fig. 8. As depicted in the figure, the thermal behavior of SAWH is highly affected by the changing tube diameter, such that as this parameter reaches higher values, the temperature in the entire region of collector, especially inside the absorber plate and the regions adjacent to this element, decreases considerably. This behavior is due to the larger surface area between the water flow and the tube's inner surface at higher values of the tube diameter. It is worth mentioning that as the density and thermal conductivity of water are significantly higher than those of the air, the potential of water flow for receiving heat transfer from the heated surface is much higher and this fact is one of the factors contributing to the decreasing of the collector temperature when water tubes with a large diameter are used in the construction of SAWH.

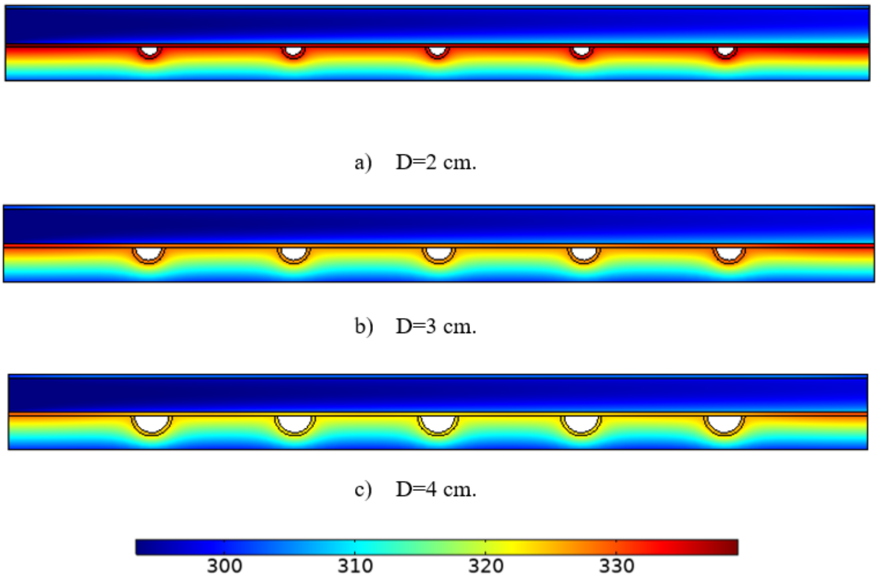

Fig. 8. Temperature contours for different diameters of water tube, $q_{sun} = 1100\ W/m^2$.

To demonstrate the benefits of the proposed SAWH, a comparison is made between the thermal behavior of this type of solar collector and the simple SAH. For this purpose, the temperature contours inside the analyzed SAH that operates under the same conditions and air mass flow rate are plotted in Fig. 9 for different values of solar heat flux. As expected, the SAH operates at very high temperatures, with the absorber's temperature being especially high. One can compare the maximum absorber's temperature of 377 K for SAH with 339 K that occurs for the proposed SAWH at the solar heat flux 1100 W/m^2.

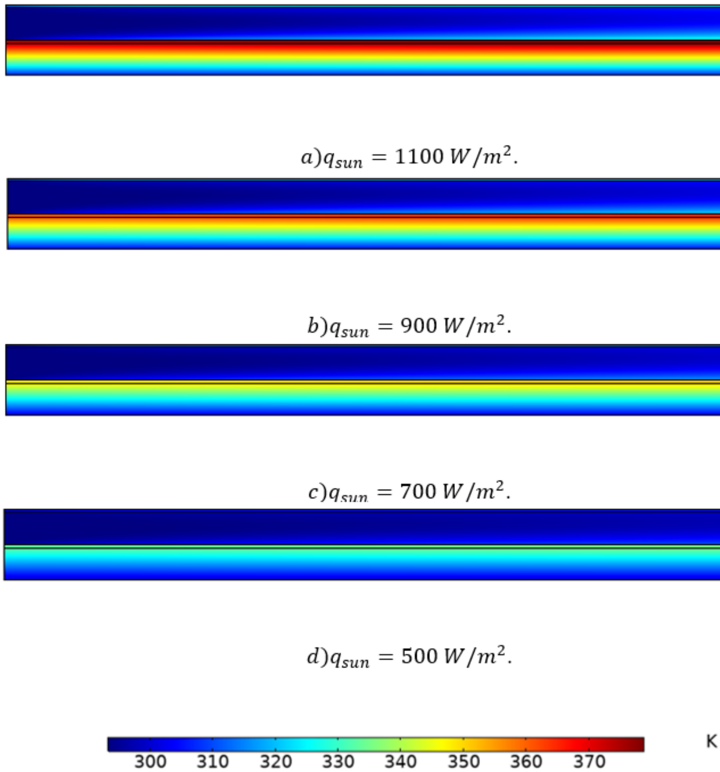

Fig: 9. Temperature contours for SAH at different levels of solar irradiation.

The temperature distribution along the insulation layer of SAH adjacent to the surrounding is plotted in Fig. 10 at four different values of the solar heat flux. This figure shows a slight increase in insulation temperature along the x-direction affected by the increase in solar heat flux. A comparison of this figure with a similar one for the SAWH again shows that the SAH operates at much higher temperatures.

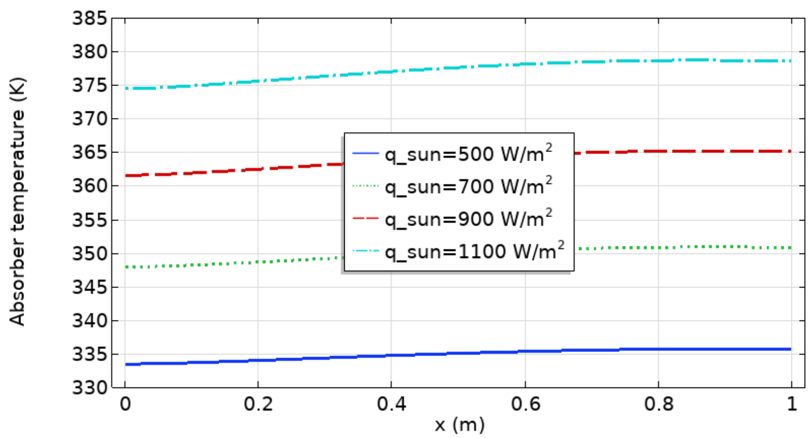

Fig. 10. Temperature distribution along the upper surface of the SAH absorber.

To verify the densities of air and water flows in receiving thermal energy from the solar collector, the rates of heat transfer into each of these working fluids, as well as the total rate of heat transfer, are plotted against the solar heat flux in Fig. 11. Moreover, one of the curves is due to the simple SAH under the same operating conditions. It is seen that for the studied test case, the rate of heat transfer into the water flow is more than twice as high as that of the air and both of these parameters have increasing trends with solar heat flux. One can compare the total heat transfer in SAWH with the simple SAH to examine the advantage of the proposed collector with the two working fluids. For example, at 1100 W/m^2 solar heat flux, the total rates of heat transfer are 790W and 400 W, for SAWH and SAH, respectively. Therefore, the efficiency of the proposed SAWH becomes approximately twice that of the SAH.

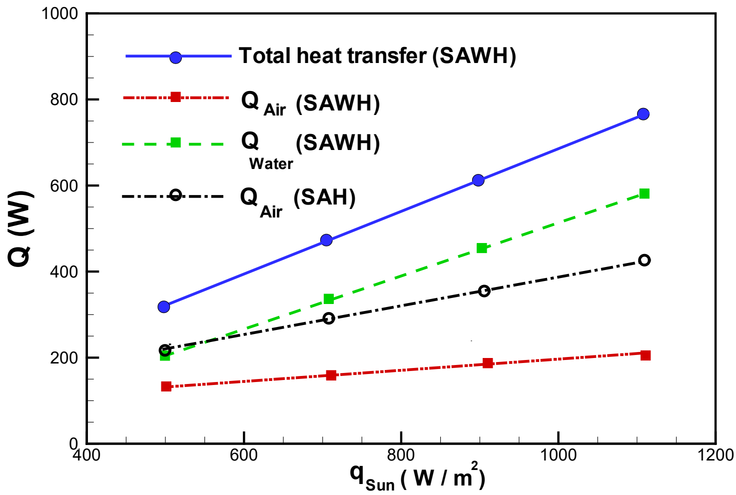

Fig. 11. Rate of heat transfer vs. Sun heat flux, D= 4 cm.

The thermal efficiency of the proposed SAWH, which shows the performance of the solar collector, has been compared with the simple SAH under similar conditions to determine the enhancement in heat transfer. Toward this end, the thermal efficiencies of these two solar collectors are computed at different levels of solar heat flux, which is illustrated in Fig. 12. Two different trends for the SAWH and SAH efficiencies are observed against the incoming solar radiation, i.e. an increasing trend for the SAWH and a decreasing one for the SAH. Thus, the responses of these solar heat exchangers are quite different. The curves plotted in Fig. 12 demonstrate that the proposed SAWH is an efficient solar collector with a considerably higher level of thermal efficiency compared to the simple SAH, especially under high solar irradiation conditions at which this improvement exceeds 1.5 times.

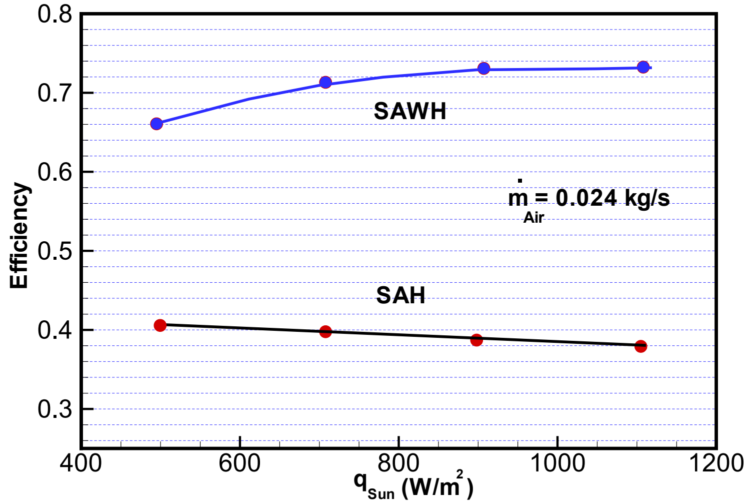

Fig. 12. Comparison of SAH and SAWH efficiencies, D=4 cm.

At the end of this section, the effect of water tube diameter on the performance of SAWH is studied by computing the rates of heat transfer into the air and water flow, a well as the thermal efficiency at different diameters, and the results are presented in Figs. 13 and 14. It can be seen from Fig. 13 that for all values of the examined diameters the rate of heat transfer into the water flow is higher than that of the air, such that as the diameter of water tubes reaches higher value, this behavior is enhanced. Finally, Fig. 14 depicts the increasing trend of thermal efficiency as the diameter of water tube increases. In addition, this figure confirms the performance improvement of the proposed SAWH under the high incoming solar heat flux conditions.

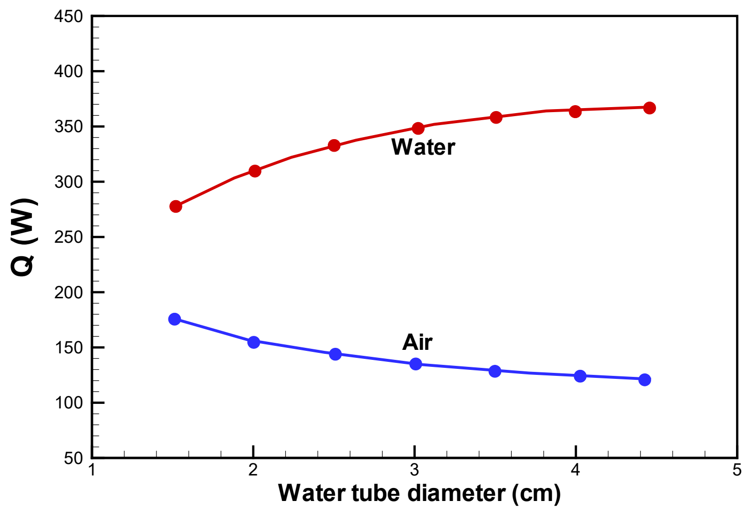

Fig. 13. Rate of heat transfer vs. diameter of water tube, $q_{sun} = 700\frac{W}{m^2}$.

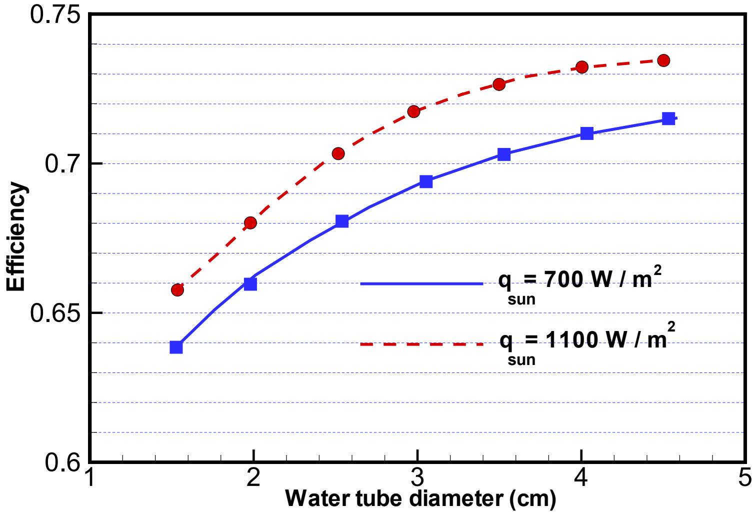

Fig. 14. Variation of SAWH efficiency vs. diameter of water tube.

4. Conclusion

This paper presents a CFD study for the purpose of verifying the performance of a new type of SAWH through the numerical solution of the airflow equations using COMSOL Multiphysics. The water tubes with a semi-circle shape of the cross section were installed under the absorber plate. The airflow above the absorber plate and the water flow inside the tubes are effectively heated with the absorbed solar heat flux. In the simulation, the region inside the water tubes is out of the two-dimensional computational domain and the convection boundary condition was employed on the water-tube interfaces. A parametric study was performed on the proposed SAWH and numerical findings showed more than 50% increase in thermal efficiency in comparison to a simple SAH for the studied test cases. This new type of solar collector can be regarded as an efficient heat exchanger, especially when heating air and water is needed for various engineering applications.

Nomenclature

A	Area (m^2)	ϵ	Turbulent dissipation (m^2/s^3)
b	Height of the air duct (m)	μ	Fluid Viscosity (Pa.s)
C_p	Specific heat (kJ/kgK)	ρ	Fluid density (kgm^{-3})
D_h	Hydraulic diameter (m)	α	Thermal diffusivity (m^2/s^2)
h	Convection coefficient (W/m^2K)	κ	Turbulence kinetic energy (m^2/s^2)
D	Outer diameter of water tubes (m)	ε	Surface emissivity
L	Length of heater (mm)	δ	Thickness (m)
p	Pressure (Pa)	Subscript	
q	Heat flux (W/m^2)	abs	absorber
Re	Reynolds number	amb	ambient
T	Temperature (K)	in	inlet
u_i	Velocity component (m/s)	out	outlet
(x, y)	Coordinates (m)	eq	equivalent
Greek symbols		ins	insulation
α_g	Glass absorptivity	m	mean
ρ_g	Glass reflectivity	w	water
τ_g	Glass transmissivity	g	glass

References

Aramesh M, Ghalebani M, Kasaeian A, Zamani H, Lorenzini G, Mahian O, Wongwises S (2019). A review of recent advances in solar cooking technology, *Renew. Energy*, 140, 419–435.

Chabane F, Noureddine M, Brima, A (2018). Experimental study of thermal efficiency of a solar air heater with an irregularity element on absorber plate, *International Journal of Heat and Technology*, 36 (2018), 855-860.

Desisa D G, Shekata G D (2020). Performance Analysis of Flat-Plate and V-groove Solar Air Heater Through CFD Simulation, *International Journal of Renewable Energy Development*, 9(3), 369-381.

Foruzan Nia F, Gandjalikhan Nassab S A, Ansari A B (2020). Numerical Simulation of Flow and Thermal Behavior of Radiating Gas Flow in Plane Solar Heaters, *J. Therm.Sci. Eng. Appl.*, 12(3), 031008.

Gandjalikhan Nassab S A (2022). Combined action of gas radiation and airfoil shaped ribs in improvement of Heater performance, *AUT Journal of Mechanical Engineering*, 6(2), 219-312.

Gandjalikhan Nassab S A (2022). Efficient design of converged ducts in solar air heaters for higher performance, *Heat and Mass Transfer*, 59, 363-375.

Gandhi B K, Singh K M (2010). Experimental and numerical investigations on flow through a wedge-shaped rib roughened duct, *Journal of the Institution of Engineers (India): Mechanical Engineering Division*, 90, 13- 18.

Ho, C D, Hsiao C F, Chang H, Tien Y E, Hong Z S (2017). Efficiency of recycling double-pass V-corrugated solar air collectors, *Energies*, 10(7) (2017), 875-883.

Hassan A, Nikbahkt A M, Welsh Z, Yarlagadda P, Fawzia S, Karim A (2022). Experimental and hermodynamic analysis of solar air dryer equipped with V-groove double pass collector: Techno-economic and exergetic measures, *Energy Conversion and Management*, 16, 100296.

Kalogirou S A (2004). Solar thermal collectors and applications, *Progress in Energy and Combustion Science*, 30, 231-295.

Launder B E, Spalding D B (1974). The numerical computation of turbulent flows, *Computer methods in applied mechanics and engineering*, 3(2), 269-289.

Nemś M, Kasperski J (2016). Experimental investigation of concentrated solar air-heater with internal multiple-fin array, *Renew. Energy*, 97, 722–730.

Rayeni A D, Gandjalikhan Nassab S A (2020). Effects of Gas Radiation on Thermal Performances of Single and Double Flow Plane Solar Heaters, *Int. J. Eng.*, 33, 1156–1166.

Sheikhnejad, Gandjalikhan Nassab S A (2021). Enhancement of solar chimney performance by passive vortex generation, *Renewable Energy*, 169, 437-450.

Singh Akshayveer A P, Kumar A, Singh O P. (2019), Designs for high flow natural convection solar air heaters, *Sol. Energy*, 193, 724–737.

Singh A P, Singh O P (2019). Thermo-hydraulic performance enhancement of convex-concave natural convection solar air heaters, *Sol. Energy*, 183,146–161.

Singh S (2020). Experimental and numerical investigations of a single and double pass porous serpentine wavy wiremesh packed bed solar air heater, *Renew. Energy*, 145, 1361–1387.

Singh S (2017). Performance evaluation of a novel solar air heater with arched absorber plate, *Renew. Energy*, 114, 879–886.

Tang L H, Chu W X, Ahmed N, Zeng M (2016). A new configuration of winglet longitudinal vortex generator to enhance heat transfer in a rectangular channel, *Applied Thermal Engineering*, 104, 74-84.